



# Coherent state path integral Monte Carlo

Riccardo Fantoni<sup>a</sup>

Dipartimento di Fisica, Università di Trieste, strada Costiera 11, 34151 Grignano (Trieste), Italy

Received 22 April 2025 / Accepted 3 October 2025

© The Author(s), under exclusive licence to EDP Sciences, SIF and Springer-Verlag GmbH Germany,  
part of Springer Nature 2025

**Abstract.** We propose a new quantum simulation method for a many-body quantum liquid of identical particles at finite (nonzero) temperature. The new scheme expands the high-temperature density matrix on the overcomplete set of single particles coherent states of John Rider Klauder instead of the usual plane waves as in conventional path integral methods. One is free to tune the elastic constant and/or the mass of the harmonic oscillator subtending the coherent states so as to maximize the computational efficiency of the algorithm. We prove that in the limit of an extremely stiff harmonic oscillator the results for the internal energy tend toward the correct expected values. Moreover, we suggest that a stiff harmonic oscillator could allow the use of larger (imaginary) timesteps. This additional degree of freedom is the characteristic feature of our new algorithm and is not available in more conventional path integral methods.

## 1 Introduction

The path integral Monte Carlo method has been used in statistical physics by a long time [1]. For fermionic systems it was worked out by V. S. Filinov [2]. A recent review by T. Dornheim et al. [3] summarizes the use of path integral Monte Carlo method for fermionic systems. Whereas Boltzmann and Bose particles can be solved exactly at least computationally, Fermi particles cannot due to the notorious *sign problem* of Feynman [4–7]. The sign problem for the ideal Fermi-gas can be solved using the so-called Brownian bridge [8].

In this work, we describe a new algorithm able to simulate a quantum liquid made of identical particles at finite temperature through the cooperation of coherent states (CS) [9–14] and the path integral Monte Carlo (PIMC) method [15]. The algorithm, which we will call coherent states path integral Monte Carlo (CSPIMC), reconstructs the equilibrium hot thermal density matrix of a many-body system of particles at each small imaginary time step thanks to the properties of the single particle coherent states that form an overcomplete set [9–14].<sup>1</sup> The coherent state is a state of minimal uncertainty which is defined to be the (unique) eigenstate of the annihilation operator of a Harmonic

Oscillator (HO) and as such it is described by a wave function whose probability distribution is a Gaussian. The information on the thermal density matrix after a sufficiently big number of sufficiently small imaginary time steps  $\tau$ , so to reach the desired finite inverse temperature  $\beta$ , is then reconstructed into a path integral through the PIMC calculation. As usual we take  $\beta = 1/k_B T = M\tau$  with  $k_B$  Boltzmann constant,  $T$  the absolute temperature,  $M$  the number of time steps discretizations between 0 and  $\beta$ , and  $\tau$  a time discretization ultraviolet cutoff.

We suggest that this way of simulating a quantum many-body system of bosons/fermions may allow to choose larger timesteps  $\tau$  which will make the Monte Carlo algorithm more efficient. This will not solve the sign problem of Feynman [4–7] which is still an open problem in statistical physics. In particular we see, as is clearly shown in Appendix C, that choosing the HO mass big enough allows to work at larger timesteps.

Our novel Quantum Monte Carlo (QMC) algorithm adds to the rich variety of similar methods for a finite temperature numerical experiment starting from the conventional *standard simulations* of D. M. Ceperley [15], passing to the *worm-algorithm* of M. Boninsegni [17], to end to the *pair-product approximation* used by E. W. Brown [18]. All these Monte Carlo methods are based on the Metropolis algorithm [19, 20] and use plane waves to expand the kinetic energy action. Attempts in the direction presented in this work can be found in literature but only applied to real time quantum dynamics rather than imaginary time statistical mechanics and for a one body problem [21].

<sup>1</sup> In particular, the completeness has been proven by Moyal [16].

**Supplementary Information** The online version contains supplementary material available at <https://doi.org/10.1140/epjd/s10053-025-01077-9>.

<sup>a</sup>e-mail: riccardo.fantoni@scuola.istruzione.it (corresponding author)

If, from one side, we do not need to specify further the *primitive approximation* [15] for the potential energy action, diagonal in position representation, on the other side, we will make a rather brute force approximation for the *kinetic action* that hinges on the peculiar properties of coherent states. We then propose a “thought” computer experiment with no ambition to carry out our own numerical experiment for fermions. But we successfully tested the new proposed kinetic energy density matrix on simulations of distinguishable Boltzmann and identical Bose free particles. These computer experiments show the approach to the correct thermodynamic value for the thermodynamic estimator of the kinetic energy in the limit of a large value for  $\xi = m_{h.o.}\omega/2$  where  $m_{h.o.}$  is the HO mass and  $\omega$  is its frequency. For example we performed a test simulation of  $16^4\text{He}$  atoms near the continuum limit ( $M = 250$ ) and compared our CSPIMC result with the one of conventional plane waves PIMC for both the kinetic energy and the potential energy. The freedom of choice of the stiffness of the HO is the characteristic feature of our new algorithm that is not present in more conventional path integral approaches. This freedom of choice of the stiffness of the HO, regulated by its mass,  $m_{h.o.}$ , and elastic constant,  $k = m_{h.o.}\omega^2$  goes together with the freedom of choice of the mass,  $m$ , of the non interacting particles. For the interacting system the mass  $m$  plays a role and one can renormalize the strength of the interaction, the coupling constant,  $v \rightarrow m\bar{v}$ , and work at fixed  $\bar{v}$ . We will see how the two masses are mingled together in the adimensional constant  $\varphi = \xi\tau/m$  that naturally appears in our formulation.

## 2 The algorithm

Let us consider a many-body system of  $N$  particles with positions  $Q = (\mathbf{q}_1, \mathbf{q}_2, \dots, \mathbf{q}_N)$  and momenta  $P = (\mathbf{p}_1, \mathbf{p}_2, \dots, \mathbf{p}_N)$  in thermal equilibrium at a finite temperature  $T$  in a volume  $\Omega$  at a density  $\rho = N/\Omega$ .

The equilibrium statistical mechanics description of the many-body fermions requires the knowledge of the thermal density matrix operator  $\hat{\rho} = \exp(-\beta\hat{H})$  where  $\hat{H}$  is the fermions Hamiltonian operator,  $\beta = 1/k_B T$  is the “inverse temperature,” and  $k_B$  is the Boltzmann constant.

The thermal density matrix satisfies to the Bloch equation

$$\frac{\partial \hat{\rho}}{\partial \beta} = -\hat{H}\hat{\rho}. \quad (2.1)$$

If we know the eigenstates and eigenvalues of the Hamiltonian,  $|\Psi_i\rangle$  and  $E_i$ , we can use the completeness of this system of orthonormal states to write the position representation of the density matrix as follows

$$\rho(Q, Q'; \beta) = \langle Q | \hat{\rho} | Q' \rangle = \sum_i \langle Q | \Psi_i \rangle e^{-\beta E_i} \langle \Psi_i | Q' \rangle. \quad (2.2)$$

Otherwise, in the high-temperature limit we can neglect terms of orders higher than one in the small  $\tau$  in the Baker–Campbell–Hausdorff formula<sup>2</sup> to find [15]

$$\rho(Q, Q'; \tau) = \langle Q | e^{-\tau\hat{H}} | Q' \rangle \approx \langle Q | e^{-\tau\hat{T}} e^{-\tau v \hat{V}} | Q' \rangle, \quad (2.3)$$

where  $\hat{H} = \hat{T} + v\hat{V} = \hat{P}^2/2m + vV(Q)$  is the Hamiltonian operator with  $\hat{T}$  the kinetic energy operator,  $\hat{V}$  the potential energy operator, with  $v$  the coupling constant,  $\hat{Q} = Q$  the positions operator,  $\hat{P} = -i(\nabla_{\mathbf{q}_1}, \nabla_{\mathbf{q}_2}, \dots, \nabla_{\mathbf{q}_N})$  the momenta operator, and  $m$  the particles mass; here and in the following we choose  $\hbar = 1$ .

Taking  $\tau = \beta/M$  with  $M$  a large integer we can then reconstruct the finite temperature density matrix using Trotter formula in the following successive ‘convolutions’ [15, 23] as usual

$$\begin{aligned} \rho(Q, Q'; \beta) &= \int \rho(Q, Q_1; \tau) \cdots \rho(Q_{M-1}, Q'; \tau) dQ_1 \\ &\cdots dQ_{M-1}. \end{aligned} \quad (2.4)$$

Since  $\hat{\rho} \approx e^{-\tau\hat{T}} e^{-\tau v \hat{V}} = \prod_{\alpha} e^{-\tau\hat{T}_{\alpha}} e^{-\tau v V_{\alpha}}$ , where  $\hat{T}_{\alpha}$  is the kinetic energy of particle  $\alpha$  and the exponential containing the potential is diagonal in position space and just a multiplicative factor, then the many-body state  $|\Upsilon_a\rangle$  factorizes into a product of single particle states  $\prod_{\alpha} |\psi_{\alpha}^a\rangle$

$$|\Upsilon_a\rangle = \prod_{\alpha=1}^N |\psi_{\alpha}^a\rangle, \quad (2.5)$$

where  $a$  labels the set of many-body states which inherit the overcompleteness of the single particles states. Here and in the following we will use Greek indexes to denote the particle label and Latin indexes to denote the label of the (over)complete single particle states.

Antisymmetrizing so to satisfy Fermi statistics (or symmetrizing so to satisfy Bose statistics), we find

$$\begin{aligned} |\Upsilon_a\rangle \langle \Upsilon_a| &= \frac{1}{N!} \sum_{\mathcal{P}} (-1)^{\mathcal{P}} \prod_{\alpha, \beta=1}^N |\psi_{\alpha}^a\rangle \langle \psi_{\mathcal{P}\beta}^a| \\ &= \frac{1}{N!} \det || |\psi_{\alpha}^a\rangle \langle \psi_{\beta}^a| ||, \end{aligned} \quad (2.6)$$

where  $\mathcal{P}$  is any of the  $N!$  permutations of the  $N$  particles.

<sup>2</sup> This is called the *primitive approximation* and is valid whenever the kinetic energy and the potential energy operators are separately bounded from below which is not the case for a two-component Coulomb liquid for which it is necessary to use the pair product density matrix as the building block [22].

Now we can take as the single particle states  $|\psi_\alpha^a\rangle$  the coherent states [9–14]

$$|\psi_\alpha^a\rangle \equiv e^{-i\mathbf{q}_a \cdot \hat{\mathbf{p}}_\alpha} e^{i\mathbf{p}_a \cdot \hat{\mathbf{q}}_\alpha} |0\rangle, \quad (2.7)$$

where  $|0\rangle$  is the ground state of the three dimensional harmonic oscillator of elastic constant  $k$  along all three dimensions<sup>3</sup>. The coordinate representation of this state is

$$\psi^a(\mathbf{q}_\alpha) \equiv \langle \mathbf{q}_\alpha | \mathbf{q}_a, \mathbf{p}_a \rangle = \left( \frac{m_{h.o.}\omega}{\pi} \right)^{3/4} e^{-\frac{m_{h.o.}\omega}{2} [\mathbf{q}_\alpha - \sqrt{\frac{2}{m_{h.o.}\omega}} \text{Re}(\mathbf{a})]^2 + i\mathbf{q}_\alpha \cdot \sqrt{2m_{h.o.}\omega} \text{Im}(\mathbf{a}) - i2\text{Re}(\mathbf{a}) \cdot \text{Im}(\mathbf{a})}, \quad (2.8)$$

$$\mathbf{a} = \frac{1}{\sqrt{2m_{h.o.}\omega}} (m_{h.o.}\omega \mathbf{q}_a + i\mathbf{p}_a), \quad (2.9)$$

where  $\omega = \sqrt{k/m_{h.o.}}$  is the angular frequency of the harmonic oscillator of elastic constant  $k$  and mass  $m_{h.o.}$ . Note that the HO, or *ghost*, coordinates,  $\mathbf{q}_a$ , are elastically bound to the particle, or *real*, coordinates,  $\mathbf{q}_\alpha$ , by a Gaussian and vice versa. In other words, the HO “ $a$ ” is centered on the particle “ $\alpha$ .” The width of the Gaussian is proportional to  $(m_{h.o.}\omega)^{-1}$  so that in the  $m_{h.o.}\omega \rightarrow \infty$  limit the ghost coordinates coincide with the particle coordinates.

This way we obtain the thermal density matrix at a finite inverse temperature  $\beta$  through the “multiple convolution” integral (2.4), but with the following high-temperature density matrix<sup>4</sup>

$$\rho(Q, Q'; \tau) \approx e^{-K(Q, Q'; \tau, m, \xi)} e^{-\tau v V(Q')} \quad (2.10)$$

$$= e^{-\tau v V(Q')} \frac{1}{N!} \sum_{\mathcal{P}} (-1)^{\mathcal{P}} \prod_{\alpha} \zeta_\alpha [\mathbf{q}_{\mathcal{P}\alpha} | \mathbf{q}'_\alpha; \tau, m, \xi], \quad (2.11)$$

where  $K$  is the kinetic part of the semiclassical action depending on the expansion of  $|\Upsilon_a\rangle$  on the single particle coherent states of Eq. (2.6),  $\zeta$  is defined in Eq. (A9) in Appendix A and its primitive approximation is determined in Eqs. (C3), of Appendix C,  $k$  is the elastic constant of the harmonic oscillator, and  $m_{h.o.}$  is its mass.

So that in the  $M \rightarrow \infty$  limit the Trotter formula (2.4) becomes a path integral made of the  $M$  high-temperature density matrices (2.11) at each time step [23].

<sup>3</sup> Our discussion will be carried out in three dimensions for definiteness but the generalization to any dimensions is straightforward.

<sup>4</sup> A general expression for the high-temperature density matrix was obtained by G. Kelbg in 1963 [24]. This expression contains the Fourier transform of the interaction potential, so it is possible to obtain high-temperature density matrices for a variety of potentials (for example, it is possible to take into account long-range interactions).

Note that if we choose an extremely stiff harmonic oscillator, i.e., one such that  $m_{h.o.}\omega \rightarrow \infty$ , then the Gaussian  $|\psi_\alpha^a(\mathbf{q})|^2$  of Eq. (2.8) reduces to a Dirac  $\delta$  centered on the position  $\mathbf{q}$  only. We suggest that this may allow the use of larger timesteps in Eq. (2.4) that reduces to the path integral. And this will increase the efficiency of the MC algorithm.

As usual in order to measure an observable  $\hat{O}$  we need to calculate  $\langle \hat{O} \rangle = \text{tr}(\hat{\rho}\hat{O})/\text{tr}(\hat{\rho})$ . This requires to impose periodic boundary conditions on the imaginary time so that  $\rho(Q, Q'; t) = \rho(Q, Q'; t + \beta)$ .

Moreover, in a simulation we want to mimic the thermodynamic limit as close as possible and this is usually obtained enforcing spatial periodic boundary conditions juxtaposing an infinite number of identical copies of the simulation box of volume  $\Omega = L_1 L_2 L_3$  along the three dimensions. This can be easily obtained by taking for each particle  $\mathbf{q}_\alpha + \mathbf{L} = \mathbf{q}_\alpha$ , i.e a periodic box. Of course as  $\Omega$  increases we will mimic the thermodynamic limit closer and closer. One usually refers to this feature of a computer experiment as the *finite size error*. This can be obtained with the expansion in coherent states by taking the following infinite sum<sup>5</sup> at the end

$$\zeta_\alpha \rightarrow \zeta_\alpha^L = \sum_{i,j=-\infty}^{\infty} \zeta_\alpha [\mathbf{q} + iL | \mathbf{q}' + jL; \tau, m, \xi], \quad (2.12)$$

where we assumed  $L_1 = L_2 = L_3 = L$  for simplicity.<sup>6</sup>

### 3 Comparison with the standard kinetic energy density matrix

We successfully performed some preliminary test simulations with our new high-temperature *coherent states* density matrix of Eq. (2.10) and compared it with the standard *plane waves* primitive approximation [15] with

$$K(Q, Q'; \tau, m) = \frac{(Q - Q')^2}{4\lambda\tau} + \frac{3N}{2} \ln(4\pi\lambda\tau), \quad (3.1)$$

and  $\lambda = 1/2m$ .

In particular, our proposed new path integral expression can be written as

<sup>5</sup> Given any function  $f(x)$  it can always be made periodic of period  $L$  by choosing  $f_L(x) = \sum_{n=-\infty}^{\infty} f(x + nL)$ .

<sup>6</sup> Note that the series (2.12) may be conditionally convergent.

$$\rho(Q_0, Q_\beta; \beta) = \frac{1}{N!} \sum_{\mathcal{P}} (-1)^{\mathcal{P}} \int_{Q_0 \rightarrow Q(t) \rightarrow \mathcal{P} Q_\beta} e^{-\int_0^\beta \frac{P_a(t)^2}{2m} + v V[Q(t)] dt} \prod_{t,t'=0}^{\beta} \prod_{\alpha=1}^N \psi_\alpha^a[\mathbf{q}(t)] \psi_\alpha^{b*}[\mathbf{q}(t')] G_{a,b} \frac{\mathcal{D}Q_a \mathcal{D}P_a}{(2\pi)^{3N}} \frac{\mathcal{D}Q_b \mathcal{D}P_b}{(2\pi)^{3N}} \mathcal{D}Q(t), \quad (3.2)$$

where  $Q_a = (\mathbf{q}_{a1}, \dots, \mathbf{q}_{aN})$  and  $P_a = (\mathbf{p}_{a1}, \dots, \mathbf{p}_{aN})$ ,  $Q_b = (\mathbf{q}_{b1}, \dots, \mathbf{q}_{b1})$  and  $P_b = (\mathbf{p}_{b1}, \dots, \mathbf{p}_{bN})$  are “ghost variables,”  $G_{a,b}$  is the normalization factor of two coherent states as defined in Eq. (A5), and  $\psi_\alpha^a(\mathbf{q}) \equiv \psi^a(\mathbf{q}_a)$  is the coherent state as defined in Eq. (2.8). In our notation,

$$\prod_{t,t'=0}^{\beta} f(t, t') = \lim_{\tau \rightarrow 0} \prod_{i=0}^{M-1} f(i\tau, (i+1)\tau), \quad (3.3)$$

is a limit productorial over the continuous imaginary time from 0 to  $\beta$ . Notice that the antisymmetrization is only necessary on the real variables: the particles positions, as usual. Also, is important to impose imaginary time and spatial periodic boundary conditions on the positions of the real and on the ghost particles, but nothing should be done on the momenta of the ghost particles. In any case the ghost particles are always naturally bound to the real particles due to the effect of the HO, so their momenta never reach infinity. All distances between real particles and between real and ghost particles should be computed using the minimum image convention. This affects both the calculation of the potential energy between real particles and also the harmonic binding between the ghost and real particles enforced by the Gaussian in Eq. (2.8) and the phase factors in those coherent states. Note that while the ghost “a” acts at time  $t$ , ghost “b” acts at time  $t + \tau$ . This is the reason why it is important to impose imaginary time periodic boundary conditions also on the ghost coordinates.

From our preliminary Metropolis [20] simulation<sup>7</sup> of

<sup>7</sup> In our simulation we choose as transition move a uniform displacement of each of the  $3MN$  real path coordinate  $\mathbf{q}_\alpha(i\tau) \rightarrow \mathbf{q}_\alpha(i\tau) + (1/2 - \eta)\Delta$  for  $\alpha = 1, \dots, N$  and  $i = 1, \dots, M$ , where  $\eta$  is a uniform pseudo-random number in  $[0, 1]$  and  $\Delta$  a fixed three-dimensional vector whose magnitude is chosen so to have acceptance ratios close to 1/2. And of each of the  $12MN$  ghost path canonical variables  $\mathbf{q}_{a_\alpha}(i\tau) \rightarrow \mathbf{q}_{a_\alpha}(i\tau) + (1/2 - \eta)\Delta$ ,  $\mathbf{p}_{a_\alpha}(i\tau) \rightarrow \mathbf{p}_{a_\alpha}(i\tau) + (1/2 - \eta)\Delta$ , and  $\mathbf{q}_{b_\alpha}(i\tau) \rightarrow \mathbf{q}_{b_\alpha}(i\tau) + (1/2 - \eta)\Delta$ ,  $\mathbf{p}_{b_\alpha}(i\tau) \rightarrow \mathbf{p}_{b_\alpha}(i\tau) + (1/2 - \eta)\Delta$ . So that the transition probability density is just a constant and drops out of the acceptance probability. A MC step consists of displacing the  $M$  timeslices of a randomly chosen ghost and real particle one by one and of a displacement of a fixed random number  $\leq M$  of timeslices, connecting two randomly chosen real particles, all at once, in a sort of “Brownian bridge,” so to realize a swap of two real particles. Here it is also necessary

distinguishable Boltzmann free particles in 3 dimensions we found good agreement for the kinetic energy,  $\langle \hat{T} \rangle = 3N/2\beta$ ,<sup>8</sup> calculated, for a single link of the ghost variables, from  $\langle \hat{T} \rangle = m(\partial \mathcal{Z}/\partial m)/\mathcal{Z}\beta$ , where  $\mathcal{Z} = \text{tr}(\hat{\rho})$  is the partition function<sup>9</sup>, so that<sup>10</sup>

$$\langle \hat{T} \rangle = \frac{3N}{2\tau} \frac{\varphi}{(1+\varphi)} \phi - \frac{\langle P_a^2(i\tau) + P_b^2(i\tau) \rangle}{4m}, \quad (3.4)$$

where we used the result of Eq. (A10) with

$$\varphi \equiv \frac{1}{2} \left( \frac{\sigma_{pw}}{\sigma_{cs}} \right)^2 = \frac{m_{h.o.}\omega\tau}{2m} = \frac{\xi\tau}{m}, \quad (3.5)$$

$$\sigma_{pw}^2 \equiv 2\lambda\tau, \quad (3.6)$$

$$\sigma_{cs}^2 \equiv 1/m_{h.o.}\omega, \quad (3.7)$$

an adimensional constant and inserted a multiplicative factor  $\phi$  to the first term of Eq. (3.4). This kinetic energy estimator reduces to the one of the standard plane waves path integral, in the  $\xi \rightarrow \infty$  limit and for  $\phi = 1$ . We see then that the characteristic parameter  $\varphi$  of our CSPIMC algorithm is just 1/2 times the ratio of the variance of the Gaussian in the plane waves case,  $\sigma_{pw}^2$ , of Eq. (3.1) and the one of the Gaussian in the coherent states case,  $\sigma_{cs}^2$ , of Eq. (2.8). We will see below that in order to have the correct measure of the internal potential energy it is necessary to take the  $\tau \rightarrow 0$  continuum limit but keeping  $\varphi = \pi/2$  constant.

#### Footnote 7 continued

to copy the same bridge also for the “a” and “b” ghosts and swap them together with the real particles.

<sup>8</sup> The result taking care of finite size,  $L$ , effects being:

$$q(\beta) = \frac{\beta}{2m} \left( \frac{2\pi}{L} \right)^2, \quad Z(\beta) = \theta_3^{3N} \left( 0, e^{-q(\beta)} \right),$$

$$\langle \hat{T} \rangle = -\frac{1}{Z(\beta)} \frac{dZ(\beta)}{d\beta},$$

where  $\theta_3$  is the elliptic theta function of third kind.

<sup>9</sup> There exist at least other three estimators for the kinetic energy [15] that are: i. The *direct* estimator obtained by taking the average of the Laplacian with the coherent states density matrix of Eq. (3.2); ii. the *thermodynamic* estimator obtained by taking the partial derivative respect to the mass or to  $\beta$ ; iii. the *virial* estimator obtained from the virial theorem.

<sup>10</sup> Note that this estimator is rather computationally cumbersome as it requires the difference of two terms that diverge in the continuum  $\tau \rightarrow 0$  limit.

Defining the efficiency of the QMC algorithm as  $\gamma_{\mathcal{O}} = 1/\sigma_{\langle \mathcal{O} \rangle} T_{\text{MC}}$ , where  $T_{\text{MC}}$  is the total computer time and  $\sigma_{\langle \mathcal{O} \rangle}$  is the estimator for the standard deviation of the measurement of the mean for property  $\mathcal{O}$ , we generally find, for the calculation through Eq. (3.4),  $\gamma_{\hat{T}}^{\text{cs}}/\gamma_{\hat{T}}^{\text{PW}} \approx 1/6$ , where  $\gamma^{\text{cs}}$  is the efficiency of the PIMC with coherent states and  $\gamma^{\text{PW}}$  is the efficiency of the PIMC with Plane Waves.

In Figure 1, we show snapshots of the real paths in each of the two schemes for a test case of  $N = 20$  free distinguishable particles of unit mass  $m = 1$ , with a density  $N/L^3 = 0.01$ , at a temperature  $T = 0.3$ , and  $m_{h.o.}\omega = 0.7$ ,  $M = 10$ . We see that the real path from our CSPIMC simulation are very similar to the ones of the standard plane wave PIMC. The result for the kinetic energy of Eq. (3.4) is comparable and agrees well with the thermodynamic limit exact result of 9, giving 9.0(7) after  $10^6$  MC steps for  $\phi \approx 6.5$ .

Choosing higher values for the parameter  $2\xi = m_{h.o.}\omega$  slows down the simulation: In order to have acceptance ratios close to 1/2 it becomes necessary to choose smaller and smaller displacements  $\Delta$ .<sup>11</sup> But, in agreement with the discussion in Appendix C, allows to use larger timesteps, which speeds up the convergence toward the continuum limit. Note that choosing higher values of  $\xi$  produces more tightly bound real paths to the ghost particles. It is important to stress that the ghost coordinates are coupled harmonically through Gaussians (see Eq. (2.8)) to the real coordinates and it is important to employ the minimum image convention when calculating the distance between the ghost particle and the real particle that enters the exponent of the Gaussian. In Table 1, we performed some test CSPIMC simulations for the case of  $N = 20$  distinguishable free particles with  $m = 1$ ,  $N/L^3 = 0.01$ ,  $T = 0.3$ ,  $M = 10$  at fixed  $\tau = 1/3$  and increasing values of  $\xi$  in order to determine the behavior of the factor  $\phi$ . We see that  $\phi$  tends toward the limiting value  $\phi_\infty \approx 2$  valid for that particular  $\tau$ . We will generally have  $\phi_\infty = \phi_\infty(\tau)$ . Moreover at a fixed value of  $\varphi$ , the simulation does not depend on the thermodynamic state,  $\rho, T$ , apart from the finite size and the continuum limit effects. We also verified that in the continuum limit,  $\tau \rightarrow 0$ , but at fixed  $\varphi$ ,  $\phi$  tends toward  $\approx \sqrt{3}$ , in Eq. (3.4), as it is shown in Table 2 for the particular case of  $\varphi = \pi/2$ .<sup>12</sup>

We performed preliminary Monte Carlo simulations for identical Bose free particles which are still exact<sup>13</sup>, within the ultraviolet cutoff  $\tau$ , the finite size effects,

<sup>11</sup> Actually the simulation “slows” down both at very high and at very low  $\xi$ .

<sup>12</sup> Note that this does not hold for the interacting system, as it is shown in the supplementary material. This is due to the fact that in the estimator of the kinetic energy there are terms depending on the interaction as shown in Ref. [15].

<sup>13</sup> In this case the expected kinetic energy in the thermodynamic limit is given by [25, 26]

$$\langle \hat{T} \rangle = \frac{3L^3}{2\beta\lambda_{dB}^3} \begin{cases} \text{Li}_{3/2+1}(1) & T < T_c \\ \text{Li}_{3/2+1}(\bar{z}) & T > T_c \end{cases}$$

**Table 1** For a test case of  $N = 20$  distinguishable free particles with  $m = 1$ ,  $N/L^3 = 0.01$ ,  $T = 0.3$ ,  $M = 10$ , for which the finite size exact thermodynamic result for the kinetic energy is  $\langle \hat{T} \rangle \approx 8.9999996090802053$ , we determined the factor  $\phi$  in Eq. (3.4) for increasing values of  $2\xi = m_{h.o.}\omega$ . One can see that  $\phi \rightarrow \phi_\infty(\tau = 1/3) \approx 2$ . In the simulations we used up to  $2 \times 10^6$  MC steps. The parameter  $\varphi = \xi\tau/m$ , whose importance for our CSPIMC has been stressed in the text, is also reported in the table

$2\xi$	$\varphi$	$\langle P_a^2(i\tau) + P_b^2(i\tau) \rangle / 4m$	$\phi$
7/10	7/60	52.2(4)	6.51
1	1/6	55.6(4)	5.02
2	1/3	59.6(4)	3.05
3	1/2	64.6(4)	2.45
4	2/3	67.7(4)	2.13
5	5/6	70.1(4)	1.93
$3\pi$	$\pi/2$	75.5(4)	1.54
10	5/3	77.6(4)	1.54
50	25/3	150.5(4)	1.98
100	50/3	157.5(4)	1.96
500	250/3	164.5(4)	1.95

**Table 2** For a test case of  $N = 20$  distinguishable free particles with  $m = 1$ ,  $N/L^3 = 0.01$ ,  $T = 0.3$  we determined the factor  $\phi$  in Eq. (3.4) for increasing values of  $M$  at fixed  $\varphi = \pi/2$  and using for  $\langle \hat{T} \rangle$  the finite size exact result of footnote 8. One can see that, in the continuum  $\tau \rightarrow 0$  limit,  $\phi \rightarrow \approx \sqrt{3}$ . The last entry reached equilibrium only after  $2 \times 10^8$  MC steps

$M$	$\langle P_a^2(i\tau) + P_b^2(i\tau) \rangle / 4m$	$\phi$
10	75.5(4)	1.54
100	827.3(4)	1.52
200	1906.8(5)	1.74
300	2867.7(5)	1.74
500	4787(1)	1.74

and the statistical errors, but require permutations sampling, which we implemented with a Monte Carlo move consisting of a swap of a pair of real particles chosen at random and of the corresponding “a” and “b” ghosts.<sup>14</sup> For example, with calculation (3.4), for  $N = 20$  identical Bose free particles of mass  $m = 1$  at a density of  $N/L^3 = 0.01$  and a temperature  $T = 0.3$

Footnote 13 continued

where  $\text{Li}_n(z)$  is the polylogarithm function,  $\lambda_{dB} = \sqrt{2\pi\beta/m}$  is the de Broglie thermal wavelength,  $T_c = (2\pi/m)[N/L^3\text{Li}_{3/2}(1)]^{2/3}$  is the critical temperature for Bose-Einstein condensation, and the fugacity  $\bar{z}$  is given by  $N/L^3 = \text{Li}_{3/2}(\bar{z})/\lambda_{dB}^3$ . Note that for Fermi free particles one just needs to replace  $\text{Li}_{3/2}(z) \rightarrow -\text{Li}_{3/2}(-z)$  and there is no condensation.

<sup>14</sup> Note that the swap move will never change the flux of permutations through the boundary conditions in a system with more than 2 particles. So it will be impossible to measure quantities like the superfluid fraction [15].

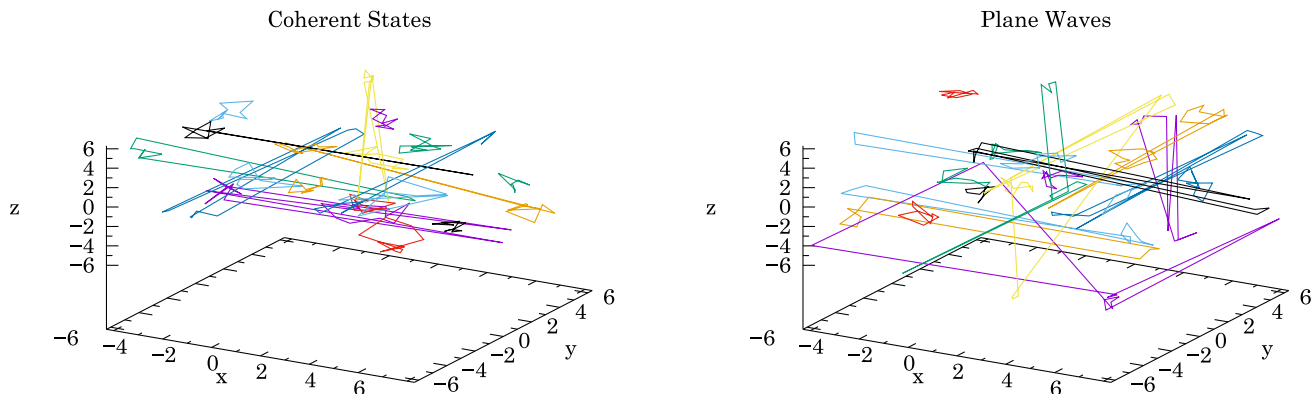


**Fig. 1** We show a comparison between equilibrium snapshots of real paths of a simulation for free distinguishable particles with our coherent states kinetic energy density matrix (left panel) and one with the standard plane waves [15] density matrix (right panel) for a test case of  $N = 20, m = 1, N/L^3 = 0.01, T = 0.3, m_{h.o.}\omega = 0.7, M = 10$  for which we found  $\langle \hat{T} \rangle = 9.0(7)$  with calculation (3.4) with  $\phi \approx 6.5$  and the exact result is  $\langle \hat{T} \rangle \approx 8.9999996090802053$ . Different (real) paths have different colors. In our CSPIMC the ghost paths are not shown but they dance nearby the real paths to which they are bound by the Gaussian of Eq. (2.8). A snapshot of the ghost paths is therefore very similar to the snapshots of the real paths. The ghost momenta at equilibrium are just centered spherically around the origin with an extent that shrinks upon choosing higher  $\xi$  values. See for example Fig. 2

with  $2\xi = 2, M = 10$  we found  $\langle \hat{T} \rangle = 7.4(7)$  with  $\phi \approx 3.03$  (compare with the values of Table 1) after  $10^6$  MC steps, when the exact thermodynamic result is  $\langle \hat{T} \rangle \approx 7.4468550673806296256$ . On the other hand identical Fermi particles are subject to the sign problem [4] and one needs to resort to some approximation even numerically with Monte Carlo. This can be realized with algorithms like for example the restricted path integral method [5].

We also performed some preliminary simulations with distinguishable Boltzmann and indistinguishable Bose particles interacting with a hard sphere, square-well [27], harmonic, Lennard-Jones [27–30], and Coulomb [31–36] pair potentials (among real particles only). For example for  $N = 16$   ${}^4\text{He}$  atoms ( $m = 0.08306 \approx 1/12 \text{ \AA}^{-2} \text{ K}^{-1}$ )<sup>15</sup> in two dimensions, a Lennard-Jones with parameters [37]  $\sigma = 2.556 \text{ \AA}, \varepsilon = 10.22 \text{ K}$  and a cutoff distance  $r_{\text{cut}} = 2.5 \text{ \AA}$  (so that  $v(r) = 0$  for  $r > r_{\text{cut}}\sigma$  without long-range corrections), at a surface density  $N/L^2 = 0.05 \text{ \AA}^{-2}$  and a temperature  $T = 1.0 \text{ K}$  with  $M = 250$ , with Boltzmann statistics and calculation (3.4) with  $2\xi = 40, \varphi = 24/25$ , we found  $\langle \hat{T} \rangle = 83(5) \text{ K}$  if  $\phi \approx 1.99$  (compare with the values of Table 1) and  $\langle \hat{V} \rangle = -83.6(3) \text{ K}$  throwing away the first  $6 \times 10^6$  equilibration MC steps and averaging over the last  $2 \times 10^6$  steps.<sup>16</sup> This should be compared with the result from conventional plane waves PIMC [38] for which we find  $\langle \hat{T} \rangle = 82.1(7) \text{ K}$  and  $\langle \hat{V} \rangle = -83.8(1) \text{ K}$  where we throw away the first  $10^6$  equilibration MC steps and average again over the last  $2 \times 10^6$ . The statistical error on the potential energy

is comparable in the two cases even if the computer time to reach a given number of steps is bigger for the CSPIMC simulation also due to the necessity to use complex arithmetic. Note that choosing larger values for  $\xi$  produces a decrease of the internal potential energy. In order to find an even better agreement between the two calculation it would be necessary to increase further  $\xi$  but keeping  $\varphi = \pi/2$  constant in the CSPIMC simulation. This requires going closer to the continuum limit  $\tau \rightarrow 0$  which will necessarily be more computationally demanding. In Fig. 2, we show a snapshot of the real and ghost variables in our CSPIMC simulation and compare it with the one for the standard plane waves PIMC.

## 4 Conclusions

We propose a new quantum simulation method for a many-body liquid. The method creates a bridge between coherent states (CS) [9–14] and conventional path integral Monte Carlo (PIMC) [15] merged together into a coherent states path integral Monte Carlo (CSPIMC) method. The idea hinges upon expanding the high-temperature density matrix on the overcomplete set of single particles coherent states of John Rider Klauder [9–14]. As the stiffness,  $\xi \equiv m_{h.o.}\omega/2$ , of the subtending harmonic oscillator (HO) varies from low values to very high values the coherent states probability distribution changes from Gaussian to Dirac delta like. We believe that going toward a more and more stiff HO the resulting extremely spiked coherent states could render the quantum Monte Carlo (QMC) simulation more and more efficient since one is allowed to work with larger timesteps.

<sup>15</sup> Here we use units where  $\hbar = k_B = 1$  so that the imaginary time has dimensions of temperature.

<sup>16</sup> Here we chose  $|\Delta| = \sqrt{2}L/100$  with acceptance ratios of  $\approx 0.5$ .

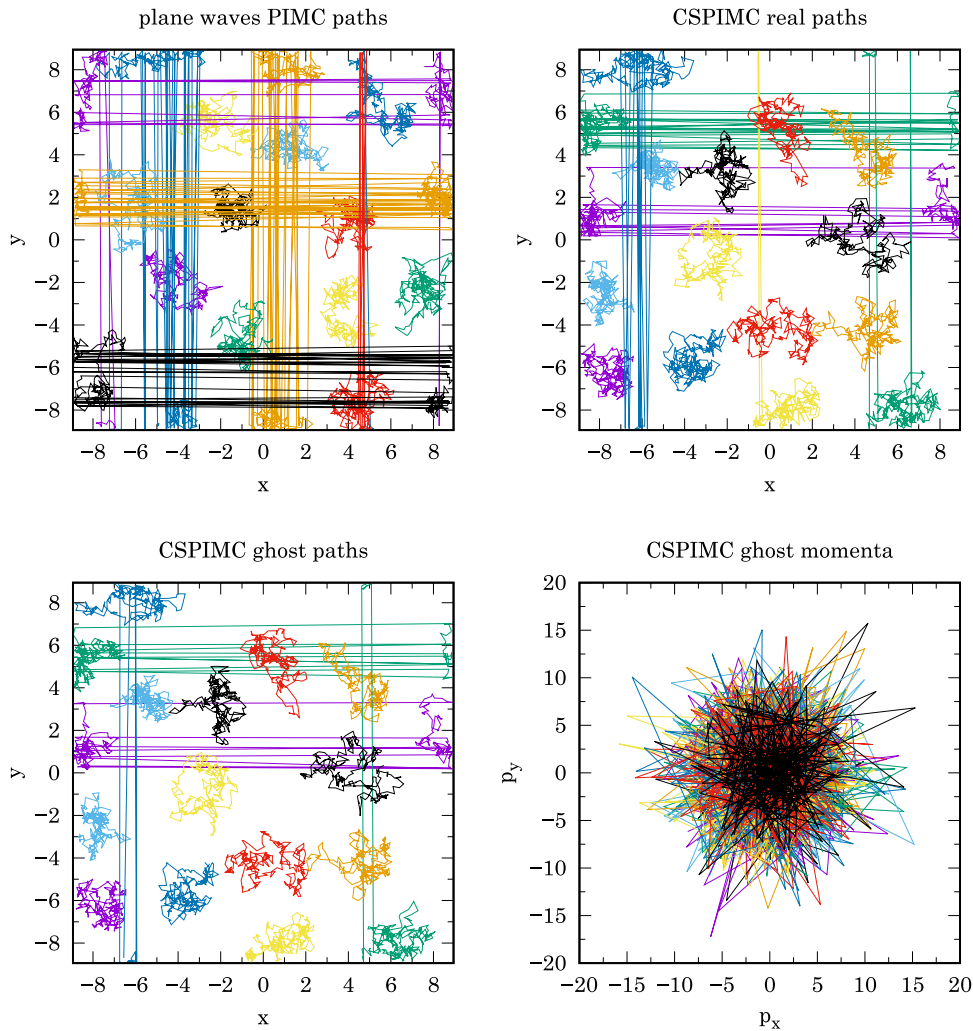


**Fig. 2** We show a snapshot at equilibrium for the paths in the plane wave PIMC and the real paths, ghost paths, and ghost momenta for the CSPIMC for  $N = 16$   ${}^4\text{He}$  atoms ( $m = 0.08306 \approx 1/12 \text{ \AA}^{-2}\text{K}^{-1}$ ) in two dimensions interacting with a Lennard-Jones pair potential with parameters [37]  $\sigma = 2.556 \text{ \AA}$ ,  $\varepsilon = 10.22 \text{ K}$  and a cutoff distance  $r_{\text{cut}} = 2.5 \text{ \AA}$ , at a density  $N/L^2 = 0.05 \text{ \AA}^{-2}$  and a temperature  $T = 1.0 \text{ K}$  with  $M = 250$ ,  $2\xi = 40$ ,  $\varphi = 24/25$  in Boltzmann statistics. Different colors refer to different real or ghost atoms

We are often interested in the ensemble thermal average  $\langle \hat{\mathcal{O}} \rangle = \text{tr}(\hat{\rho}\hat{\mathcal{O}})/\text{tr}(\hat{\rho})$  of an observable  $\mathcal{O}$  at a given finite inverse temperature  $\beta$ . Using the coordinate representation for the density matrix  $\hat{\rho}$ , as in Eq. (2.4), we arrive to the sought for path integral expression with closed paths in periodic imaginary time, such that  $t + \beta = t$  which must be enforced due to the trace in the thermal average. A key ingredient is the high-temperature density matrix at a small inverse temperature  $\tau$ . This is made up of two pieces: a new kinetic energy action and the usual diagonal potential energy action. We find the explicit analytic primitive approximation form of the kinetic energy action. Being the kinetic energy density matrix a product of single particles kinetic energy operators it is possible to expand it in the overcomplete set of single particles Klauder coherent states. The result is summarized into the  $\zeta$  function of Eqs. (C3). In particular, we see from that

equation that is necessary to introduce some “ghost variables” along the path integral whose expression becomes the one in Eq. (3.2). From this equation we see how the action (compare with Eq. (1.1) of Ref. [5]) now has a kinetic energy part where the ghost variables (coordinates and momenta) play a role and the potential energy part that remains the one of the real particles, as usual. Therefore it is important to impose periodic boundary conditions on imaginary time and on space both for the real and ghost coordinates but not on the ghost momenta. Of course the distance between particle-particle and ghost particle should also be computed using the minimum image convention.

Our calculation shows that for a very stiff HO the high-temperature kinetic energy density matrix tends to become extremely peaked (see Fig. 3). We suggest that this could allow an improvement in the efficiency  $\gamma_{\mathcal{O}}$ . Of course it is necessary to choose  $\tau$  small enough so

that our approximation (B1) does not break down. Our preliminary simulations on distinguishable free particles, (see Fig. 1) confirm this. In particular, we showed that increasing  $m_{h.o.}\omega$  the result for the kinetic energy tends to the correct limiting value in accord with the exact finite size result from thermodynamics. So we are facing a compromise between the slowing down due to the choice of a higher  $m_{h.o.}\omega$  and the speeding up due to the opportunity to choose larger timesteps  $\tau$ . It could be possible to have comparable efficiencies by choosing larger timesteps. Nonetheless, our new algorithm still results less efficient than the standard one employing plane waves and with longer equilibration times. Even if the increase in the computer time that we face in our CSPIMC respect to the standard plane waves PIMC is due to the necessity to use complex arithmetic in the former.

So, summarizing, in our new CSPIMC scheme we require as usual the two limiting procedures: i. thermodynamic limit,  $L \rightarrow \infty$  with the density  $N/L^3$  kept constant; ii. continuum limit,  $M \rightarrow \infty$  with the temperature  $T = 1/k_B M\tau$  kept constant<sup>17</sup>. But the novelty respect to more conventional path integral methods is the new degree of freedom offered by the mass,  $m_{h.o.}$ , and elastic constant,  $k = m_{h.o.}\omega^2$ , of the harmonic oscillator defining the coherent states overcomplete basis set. In the limit of a very stiff harmonic oscillator,  $\xi \equiv m_{h.o.}\omega/2 \rightarrow \infty$ , the harmonic oscillator ghost coordinates coincides with the real particles coordinates and CSPIMC reduces to conventional plane waves PIMC. For finite values of  $m_{h.o.}\omega$  the real particles are elastically bound to the ghost particles and they are mutually influenced: The ghost pulls the particle and the particle pushes the ghost! In the action the kinetic energy is that of the ghosts but the potential energy is that among the particles. In approaching the continuum limit it is necessary to keep  $\varphi \equiv \xi\tau/m = \pi/2$  constant in order to have the correct internal potential energy measure,  $\varphi$  being the characteristic parameter for our CSPIMC algorithm. We then see that with our algorithm we can relax the continuum  $\tau \rightarrow 0$  limit by choosing  $\xi \rightarrow \infty$ .

We will worry about the mathematical rigor of the primitive approximation proposed here, as described in Appendix C, or about its refinements [15], in future more specialized works. This could be important also to further increase the computational efficiency of the numerical experiment.

The use of coherent states in a quantum many-body calculation could eventually lead to the formulation of a quantum version of a molecular dynamics simulation. Klauder in Ref. [10] determines generalized relation between quantum and classical dynamics using the coherent states formalism that he calls continuous representation. As is shown in Section 2.B of that reference such correspondence is only *inexact* if the Hamiltonian is not linear or quadratic in the canonical variable. But some progress can be made for Hamiltonians where the potential energy is just a function of the positions. This was the main motivation that triggered the development of the present work on a Monte Carlo simulation instead, but we intend to reconsider the challenge of the development of a quantum molecular dynamic computer experiment soon enough. This would result in a unifying formalism for a quantum many-body computational experiment.

Additional support to the findings reported in this work is contained in the supplementary material where the listing of the FORTRAN code used in the CSPIMC simulation is given.

**Acknowledgements** I would like to thank prof. John Rider Klauder for transmitting me the passion for coherent states and all the ‘family’ of the Physics Department in Gainesville at the University of Florida which invited me to participate at the Memorial Conference held on 15 February 2025 in honor of the professor path in life and science. The professor passed away on 24 October 2024 at 92 years of age. I would like also to thank prof. Saverio Moroni for his support in creating the computer code for the plane wave simulations for  ${}^4\text{He}$  in Bose statistics.

**Funding** None declared.

**Data availability** The manuscript has associated data in a data repository.

#### Declarations

**Conflict of interest** None declared.

<sup>17</sup> Of course this limit is superfluous for a non interacting system where one always just needs two timeslices.

## Appendix A Determination of $K$ in Eq. (2.10)

From Eq. (2.3) and inserting the resolution of the identity from Eq. (2.6) in terms of the complete set of coherent states two times we find

$$\rho(Q, Q'; \tau) \approx \frac{1}{N!^2} \sum_{a,b} \langle Q | \det || |\psi_\alpha^a\rangle\langle\psi_\beta^a| || e^{-\tau\hat{T}} \det || |\psi_\alpha^b\rangle\langle\psi_\beta^b| || |Q'\rangle e^{-\tau v V(Q')}, \quad (\text{A1})$$

here

$$\sum_{a,b} \dots \rightarrow \int \dots \frac{d\mathbf{q}_a d\mathbf{p}_a}{(2\pi)^3} \frac{d\mathbf{q}_b d\mathbf{p}_b}{(2\pi)^3}. \quad (\text{A2})$$

Now the two antisymmetrizations are redundant and one can safely keep just one of the two. We then find

$$\begin{aligned} \rho(Q, Q'; \tau) &\approx \frac{1}{N!} \sum_{\mathcal{P}} (-1)^{\mathcal{P}} \sum_{a,b} \prod_{\alpha,\beta} \langle \mathbf{q}_1, \dots, \mathbf{q}_N | \psi_{\mathcal{P}\alpha}^a \rangle \langle \psi_\beta^a | e^{-\tau\hat{T}} | \psi_\alpha^b \rangle \langle \psi_\beta^b | Q' \rangle e^{-\tau v V(Q')} \\ &= \frac{1}{N!} \sum_{\mathcal{P}} (-1)^{\mathcal{P}} \sum_{a,b} \prod_{\alpha} \langle \mathbf{q}_{\mathcal{P}1}, \dots, \mathbf{q}_{\mathcal{P}N} | \psi_{\alpha}^a \rangle \langle \psi_{\alpha}^a | e^{-\tau\hat{T}_{\alpha}} | \psi_{\alpha}^b \rangle \langle \psi_{\alpha}^b | Q' \rangle e^{-\tau v V(Q')}, \end{aligned} \quad (\text{A3})$$

where we decided to keep the antisymmetrization only on the left particles positions and in the last equality we used the resolution of the identity (intimately connected to the Segal-Bargmann transform)  $\sum_a |\psi_\alpha^a\rangle\langle\psi_\beta^a| = \delta_{\alpha,\beta}$ . We will also use the following orthogonality condition among single particle coherent states

$$\langle \psi_\beta^a | \psi_\alpha^b \rangle = G_{a,b} \delta_{\alpha,\beta}, \quad (\text{A4})$$

where  $\delta$  is a Kronecker delta symbol and

$$G_{a,b} = e^{-\frac{1}{2}(|a|^2 + |b|^2) + a^* \cdot b + \frac{i}{2}(q_a \cdot p_a - q_b \cdot p_b)}, \quad (\text{A5})$$

$$a = \frac{1}{\sqrt{2m_{h.o.}\omega}}(m_{h.o.}\omega q_a + ip_a), \quad (\text{A6})$$

$$b = \frac{1}{\sqrt{2m_{h.o.}\omega}}(m_{h.o.}\omega q_b + ip_b), \quad (\text{A7})$$

here  $\omega = \sqrt{k/m_{h.o.}}$  is the angular frequency of the harmonic oscillator of elastic constant  $k$  and mass  $m_{h.o.}$ .

We then find from Eq. (2.10)

$$\equiv \frac{1}{N!} \sum_{\mathcal{P}} (-1)^{\mathcal{P}} \prod_{\alpha} \zeta_{\alpha} [\mathbf{q}_{\mathcal{P}\alpha} | \mathbf{q}'_{\alpha}; \tau, m, \xi], \quad (\text{A9})$$

where  $\langle Q | \psi^a \rangle = \langle Q | \mathbf{q}_a, \mathbf{p}_a \rangle$  is the position representation of the single particle coherent state. The element

$\langle \psi_\alpha^a | e^{-\tau\hat{T}_{\alpha}} | \psi_\alpha^b \rangle$  is found in Appendix B. The function  $\zeta$  is defined in Eq. (A9) and determined in Appendix C.

It is important to extract the diagonal part of the high-temperature kinetic density matrix of the distinguishable particles. From Eq. (A8) and using the approximation of Eq. (B2) and the definitions of Eqs. (2.8) and (A5) we readily find

$$e^{-K(Q, Q'; \tau, m, \xi)} = \left[ \frac{\xi}{2\sqrt{\pi\xi(1+2\xi\lambda\tau)}} \right]^{3N}, \quad (\text{A10})$$

where  $\xi = m_{h.o.}\omega/2$ . Note that in the  $\xi \rightarrow \infty$  limit we find the usual result for plane waves  $(4\pi\lambda\tau)^{-3N/2}$  but times  $2^{-3N/2}$ .

## Appendix B Calculation of the element of Eq. (A8)

We want here calculate explicitly the matrix element of Eq. (A8). We can then think that we find

$$\langle \psi_\alpha^a | e^{-\tau\hat{T}_{\alpha}} | \psi_\alpha^b \rangle \approx \langle \psi_\alpha^a | \psi_\alpha^b \rangle e^{-\tau(p_a^2 + p_b^2)/4m} \quad (\text{B1})$$

$$= G_{a,b} e^{-\tau(p_a^2 + p_b^2)/4m}, \quad (\text{B2})$$

where in the second equality we used the exact normalization factor of Eq. (A5). Note that the symmetriza-

$$e^{-K(Q, Q'; \tau, m, \xi)} = \frac{1}{N!} \sum_{\mathcal{P}} (-1)^{\mathcal{P}} \prod_{\alpha} \sum_{a,b} \langle \mathbf{q}_{\mathcal{P}1}, \dots, \mathbf{q}_{\mathcal{P}N} | \psi_{\alpha}^a \rangle \langle \psi_{\alpha}^a | e^{-\tau\hat{p}_{\alpha}^2/2m} | \psi_{\alpha}^b \rangle \langle \psi_{\alpha}^b | \mathbf{q}'_1, \dots, \mathbf{q}'_N \rangle \quad (\text{A8})$$

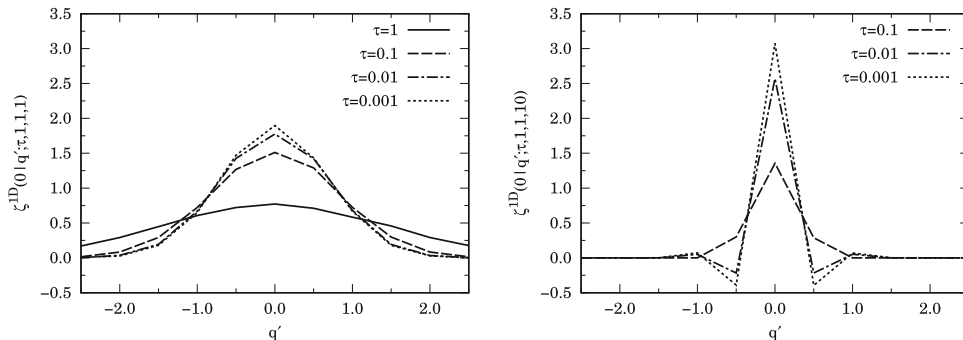


**Fig. 3** We show the one dimensional  $\zeta^{1D}(q|q'; \tau, m, \xi)$  calculated with a Monte Carlo scheme using  $10^7$  (with the related statistical error) sampling points and choosing smaller and smaller timestep  $\tau$ . All the four integrations over the ghost variables  $(q_a, p_a)$  and  $(q_b, p_b)$  were chosen in the interval  $[-l, l]$ ,  $l = 10$  (with the related finite size error). On the left  $m_{h.o.} = 1$  on the right  $m_{h.o.} = 10$ . Note that the slight negative values for the high  $m_{h.o.}$  and small  $\tau$  case are numerical artifacts due to the finite size,  $l < \infty$ , error

tion in the kinetic energy at the exponent is crucial in the Monte Carlo. Also we decided to use the “a” and “b” momenta at the same imaginary time unlike the two ghosts coordinates where “a” is at time  $t$  and “b” at time  $t + \tau$ . The approximation in Eq. (B1) is rather suggestive and extremely simple. We believe that it will be “washed away” for small  $\tau$  as our preliminary simulation confirms. In any case this is a rather subtle issue that still asks for mathematical rigor. Mathematically we need to prove that this high-temperature matrix element should be able to reconstruct the finite temperature density matrix as an exact path integral [39].

## Appendix C Determination of $\zeta$

We have from the definition in Eq. (A9)

$$\zeta_\alpha[\mathbf{q}|q'; \tau, m, \xi] \equiv \sum_{a,b} \langle \mathbf{q} | \psi_\alpha^a \rangle \langle \psi_\alpha^a | e^{-\tau \hat{T}_\alpha} | \psi_\alpha^b \rangle \langle \psi_\alpha^b | \mathbf{q}' \rangle \quad (\text{C1})$$

$$= \int \frac{dq_a dp_a}{(2\pi)^3} \frac{dq_b dp_b}{(2\pi)^3} \psi_\alpha^a(\mathbf{q}) \psi_\alpha^{b*}(q') \langle \psi_\alpha^a | e^{-\tau \hat{T}_\alpha} | \psi_\alpha^b \rangle \quad (\text{C2})$$

$$\approx \int \frac{dq_a dp_a}{(2\pi)^3} \frac{dq_b dp_b}{(2\pi)^3} \psi_\alpha^a(\mathbf{q}) \psi_\alpha^{b*}(q') G_{a,b} e^{-\tau(p_a^2 + p_b^2)/4m}, \quad (\text{C3})$$

where  $\psi_\alpha^a(\mathbf{q})$  is the coordinate representation of the single  $\alpha$  particle coherent state of Eq. (2.8) and the density matrix  $\langle \psi_\alpha^a | e^{-\tau \hat{T}_\alpha} | \psi_\alpha^b \rangle$  has been approximated in Eq. (B2) of Appendix B. Eq. (C3) can be integrated with a simple Monte Carlo scheme (see Fig. 3) and this will give us a primitive approximation for  $\zeta$ . These additional integrations over  $(\mathbf{q}_a, \mathbf{p}_a)$  and  $(\mathbf{q}_b, \mathbf{p}_b)$  must be carried out at each timestep but Monte Carlo will not suffer critically since it is designed to treat highly multidimensional integrals. We will then reach a path integral both on the particles positions and on *ghost variables* at two next time steps as shown in Eq. (3.2). In particular instead of the usual  $3MN$  discretized multidimensional path integral, we will now deal with a  $5 \times (3MN)$  multidimensional path integral. The ghost

variables are the canonical pair of labels from the continuous representation of Klauder and can be treated as canonical variables of *ghost particles* with momenta that should not be limited employing periodic boundary conditions. In the  $\tau \rightarrow 0$  limit, also within the approximation (B1), we will have,

$$\zeta_\alpha[\mathbf{q}|q'; \tau, m, \xi] \xrightarrow{\tau \rightarrow 0} \langle \mathbf{q} | \mathbf{q}' \rangle = \delta(\mathbf{q} - \mathbf{q}'), \quad (\text{C4})$$

where  $\delta$  is a Dirac delta function. The  $\tau \rightarrow 0$  limit washes away the  $k, m_{h.o.}$  dependence. On the other hand choosing a stiff harmonic oscillator, i.e., one with a high mass, the  $\zeta$  function width diminishes, as shown in Fig. 3. This will allow to choose bigger timesteps in the path integral, thereby reducing the computational cost.

## References

1. L.D. Fosdick, H.F. Jordan, Path-integral calculation of the two-particle Slater sum for  ${}^4\text{He}$ . *Phys. Rev.* **143**, 58 (1966). <https://doi.org/10.1103/PhysRev.143.58>
2. V. Filinov, G. Norman, On phase transition in a non-ideal plasma. *Phys. Lett. A* **55**, 219 (1975). [https://doi.org/10.1016/0375-9601\(75\)90719-7](https://doi.org/10.1016/0375-9601(75)90719-7)
3. T. Dornheim, S. Groth, M. Bonitz, The uniform electron gas at warm dense matter conditions. *Phys. Reports* **744**, 1 (2018). <https://doi.org/10.1016/j.physrep.2018.04.001>
4. D.M. Ceperley, Fermion Nodes. *J. Stat. Phys.* **63**, 1237 (1991). <https://doi.org/10.1007/BF01030009>
5. D.M. Ceperley, Path integral Monte Carlo methods for fermions, in booktitle Monte Carlo and Molecular Dynamics of Condensed Matter Systems, editor edited by editor K. Binder and editor G. Ciccotti (Editrice Compositori, Bologna, Italy, 1996) 4
6. R.P. Feynman, Simulating physics with computers. *Int. J. Theor. Phys.* **21**, 467 (1982)
7. R.P. Feynman, A.R. Hibbs, D.F. Styer, Quantum mechanics and path integrals, edition emended ed. (Dover Publications, 2010) 292–293

8. V.S. Filinov, A.S. Larkin, P.R. Levashov, Uniform electron gas at finite temperature by fermionic-path-integral Monte Carlo simulations. *Phys. Rev. E* **102**, 033203 (2020). <https://doi.org/10.1103/PhysRevE.102.033203>
9. J.R. Klauder, Continuous-Representation Theory. I. Postulates of Continuous-Representation Theory,. *J. Math. Phys.* **4**, 1055 (1963). <https://doi.org/10.1063/1.1704034>
10. J.R. Klauder, Continuous-Representation Theory II. generalized relation between quantum and classical dynamics,. *J. Math. Phys.* **4**, 1058 (1963). <https://doi.org/10.1063/1.1704035>
11. J.R. Klauder, Continuous-Representation Theory III. on functional quantization of classical systems,. *J. Math. Phys.* **5**, 177 (1964). <https://doi.org/10.1063/1.1704107>
12. J. McKenna, J.R. Klauder, Continuous-Representation Theory IV. on functional quantization of classical systems,. *J. Math. Phys.* **5**, 878 (1964). <https://doi.org/10.1063/1.1704190>
13. J.R. Klauder, J. McKenna, Continuous-Representation Theory. V. construction of a class of scalar boson field continuous representations. *J. Math. Phys.* **6**, 68 (1965). <https://doi.org/10.1063/1.1704265>
14. J.R. Klauder, B. Skagerstam, Coherent states (World Scientific, Singapore, 1985)
15. D.M. Ceperley, Path integrals in the theory of condensed helium. *Rev. Mod. Phys.* **67**, 279 (1995). <https://doi.org/10.1103/RevModPhys.67.279>
16. J.E. Moyal, Quantum mechanics as a statistical theory. *Proc. Cambridge Phil. Soc.* **45**, 99 (1949). <https://doi.org/10.1017/S0305004100000487>
17. M. Boninsegni, N. Prokof'ev, B. Svistunov, Worm algorithm for continuous-space path integral Monte Carlo simulations. *Phys. Rev. Lett.* **96**, 070601 (2006). <https://doi.org/10.1103/PhysRevLett.96.070601>
18. E.W. Brown, B.K. Clark, J.L. DuBois, D.M. Ceperley, path-integral Monte Carlo simulation of the warm dense homogeneous electron gas. *Phys. Rev. Lett.* **110**, 146405 (2013). <https://doi.org/10.1103/PhysRevLett.110.146405>
19. N. Metropolis, A.W. Rosenbluth, M.N. Rosenbluth, A.M. Teller, E. Teller, Equation of state calculations by fast computing machines. *J. Chem. Phys.* **1087**, 21 (1953)
20. M.H. Kalos, P.A. Whitlock, Monte Carlo Methods (John Wiley & Sons Inc., New York, 1986)
21. T. L. Marchioro II and Thomas L. Beck, Monte Carlo evaluation of real time coherent state path integrals, *J. Chem. Phys.* **96**, 2966 (1992). <https://doi.org/10.1063/1.461994>
22. E.L. Pollock, Properties and computation of the Coulomb pair density matrix. *Computer Physics Communications* **52**, 49 (1988). [https://doi.org/10.1016/0010-4655\(88\)90171-3](https://doi.org/10.1016/0010-4655(88)90171-3)
23. H.F. Trotter, On the Product of Semi-Groups of Operators. *Proc. Am. Math. Soc.* **10**, 545 (1959). <https://doi.org/10.1090/S0002-9939-1959-0108732-6>
24. G. Kelbg, Theorie des Quanten-Plasmas. *Ann. Phys.* **467**, 219 (1963). <https://doi.org/10.1002/andp.19634670308>
25. L.D. Landau, E.M. Lifshitz, Statistical physics, series course of theoretical physics, Vol. 5 (Butterworth Heinemann, 1951) translated from the Russian by J.B. Sykes and M.J. Kearsley, edited by E.M. Lifshitz and L.P. Pitaevskii
26. R.P. Feynman, Statistical mechanics: a set of lectures, series Frontiers in Physics, Vol. 36 (W.A. Benjamin, Inc., 1972) notes taken by R. Kikuchi and H.A. Feiveson, edited by Jacob Shaham
27. R. Fantoni, Gas-liquid coexistence for the bosons square-well fluid and the  ${}^4\text{He}$  binodal anomaly. *Phys. Rev. E* **90**, 020102(R) (2014). <https://doi.org/10.1103/PhysRevE.90.020102>
28. R. Fantoni, S. Moroni, Quantum Gibbs ensemble Monte Carlo. *J. Chem. Phys.* **141**, 114110 (2014). <https://doi.org/10.1063/1.4895974>
29. R. Fantoni, Two-phase coexistence for hydrogen-helium mixtures. *Phys. Rev. E* **92**, 012133 (2015). <https://doi.org/10.1103/PhysRevE.92.012133>
30. R. Fantoni, Supercooled superfluids in Monte Carlo simulations. *Eur. Phys. J. B* **89**, 1 (2016). <https://doi.org/10.1140/epjb/e2016-60917-9>
31. R. Fantoni, Radial distribution function in a diffusion Monte Carlo simulation of a Fermion fluid between the ideal gas and the Jellium model. *Eur. Phys. J. B* **86**, 286 (2013). <https://doi.org/10.1140/epjb/e2013-40204-3>
32. R. Fantoni, Two component boson-fermion plasma at finite temperature. *Int. J. Mod. Phys. C* **29**, 1850028 (2018). <https://doi.org/10.1142/S0129183118500286>
33. R. Fantoni, One-component fermion plasma on a sphere at finite temperature. *Int. J. Mod. Phys. C* **29**, 1850064 (2018). <https://doi.org/10.1142/S012918311850064X>
34. R. Fantoni, Jellium at finite temperature using the restricted worm algorithm. *Eur. Phys. J. B* **94**, 63 (2021). <https://doi.org/10.1140/epjb/s10051-021-00078-y>
35. R. Fantoni, Jellium at finite temperature. *Mol. Phys.* **120**, 4 (2021). <https://doi.org/10.1080/00268976.2021.1996648>
36. R. Fantoni, One-component fermion plasma on a sphere at finite temperature. The anisotropy in the paths conformations. *J. Stat. Mech.* (2023). <https://doi.org/10.1088/1742-5468/aceb54>
37. W.L. McMillan, Ground state of liquid  ${}^4\text{He}$ . *Phys. Rev.* **138**, 442 (1964). <https://doi.org/10.1103/PhysRev.138.A442>
38. M.C. Gordillo, D.M. Ceperley, Path-integral calculation of the two-dimensional  ${}^4\text{He}$  phase diagram. *Phys. Rev. B* **58**, 6447 (1998). <https://doi.org/10.1103/PhysRevB.58.6447>
39. L.S. Schulman, *Techniques and applications of path integration* (John Wiley & Sons Technion, Haifa, Israel, 1981)

Springer Nature or its licensor (e.g. a society or other partner) holds exclusive rights to this article under a publishing agreement with the author(s) or other rightsholder(s); author self-archiving of the accepted manuscript version of this article is solely governed by the terms of such publishing agreement and applicable law.